# Synoptic Wave Perturbations and Convective Systems over Equatorial Africa

Hanh Nguyen and Jean Philippe Duvel

Laboratoire de Météorologie Dynamique, ENS, Paris, France

Submitted to the *Journal of Climate*

Decembre 2007

Revised April 2008

**Corresponding author address:**
Dr. Jean-Philippe Duvel,
Laboratoire de Météorologie Dynamique,
Ecole Normale Supérieure,
24 rue Lhomond, F-75231
Paris Cedex 05, France.
E-mail: jpduvel@lmd.ens.fr

**Abstract**

The synoptic variability over Equatorial Africa is associated with oscillations of the convection with periods between 3 and 6 days. In March and April, when the Inter-Tropical Convergence Zone (ITCZ) migrates northward and crosses Equatorial Africa, this periodic behavior is most pronounced with a marked peak at 5-6 days. Robust horizontal and vertical patterns, consistent with a convectively coupled Kelvin wave, can be extracted by a simple composite technique based only on the phase of the convective oscillations over Equatorial Africa. The composite reveals differences between continental and adjacent oceanic regions. Over the continent, the stronger oscillation of the convection is associated with larger temperature and moisture anomalies near the surface, suggesting an influence of diabatic processes on the amplitude of the perturbations. Some convective events over Equatorial Africa are triggered by waves propagating eastward over the equatorial Atlantic. However, this cannot explain the robust periodic behavior observed over Equatorial Africa since the convective variability over the Amazon basin and the equatorial Atlantic have different spectral characteristics with no marked peak at 5-6 days in March and April.

The mesoscale convective systems embedded in these synoptic disturbances are studied using satellite brightness temperature at higher spatial (0.5°) and temporal (3 hours) resolution than the OLR (respectively 2.5° and daily average). We inspect the diurnal and the wave modulations of occurrence, size and life cycle of the mesoscale convective systems. These systems are generated preferentially over the western slopes of the Rift Valley highlands. They propagate west southwestward over the Congo basin where they reach their maximum size. The 5- to 6-day perturbations do not modify notably the diurnal triggering of convective systems but rather their development into larger organized convection, especially over the Congo basin. The implication of these results for understanding the physical source of these 5- to 6-day perturbations is discussed.

## 1. Introduction

Convection embedded in the Inter-Tropical Convergence Zone (ITCZ) fluctuates over a large spectrum of space and time scales. Generally, a relatively small part of this variability is directly associated with organized synoptic scale (i.e. ~2-10 days) dynamical perturbations. Equatorially trapped waves (Matsuno 1966), such as Kelvin waves, typically represent less than 10% of planetary to synoptic-scale variance of Outgoing Longwave Radiation (OLR) for most of the tropics (Wheeler and Kiladis 1999). Nevertheless, for specific regions and seasons, perturbations of deep convection associated with synoptic scale dynamical perturbations may significantly impact weather variability and predictability. For example, African Easterly Waves (AEWs) play a large role in the synoptic variability of the deep convection over West Africa in boreal summer (e.g. Reed et al. 1977; Payne and McGarry 1977; Duvel 1990; Diedhiou et al. 1999; Fink and Reiner 2003; Kiladis et al. 2006; Mekonnen et al. 2006). It was shown that AEWs modulate the convection, mostly by promoting large mesoscale convective systems (MCSs) in the trough of the wave (see e.g. Machado et al. 1993). This modulation of deep convection is not only a response to synoptic dynamical forcing. Indeed, the associated convective heating perturbation gives a positive feedback to the synoptic perturbation, forming a coupled system (Wheeler and Kiladis 1999, Yang et al. 2003). A better knowledge of the relationship between synoptic dynamical perturbations and deep convection is therefore essential to improve short- to medium-range weather forecasts in regions where such coupling exists.

The question is especially pertinent over Central Africa, an inhabited equatorial continental region where equatorially trapped waves may strongly influence weather patterns and synoptic forecasts. In this paper, “Central Africa” or “Equatorial Africa” refers to the continental region (mainly the Congo basin) located near the equator, west of the Rift Valley highlands (Fig.1). The ITCZ crosses the equator twice a year over Central Africa. This equatorial location of the ITCZ may efficiently reinforce Kelvin waves that are theoretically associated with a geopotential (or convective heating) perturbation centered at the equator. There is evidence of stronger variance in the Kelvin wave space-time spectral domain for a region extending from the Amazon basin to equatorial Africa (Wheeler and Kiladis 1999), especially for the November to April season. Wang and Fu (2007) indeed show convectively coupled Kelvin-like waves forming over the Amazon during boreal spring and propagating over the Atlantic. Some strong episodes over the Amazon, which could themselves be triggered by perturbations coming from the Pacific (Liebmann et al. 2008), could also trigger convection over Central Africa. However, results reported in Wang and Fu (2007) suggest that these Amazonian perturbations are not the only source of synoptic variability over Equatorial Africa. The strong Kelvin signal during boreal spring over both regions could thus also be related to the equatorial position of the ITCZ favoring the local development of convectively coupled disturbances. This is an important topic that will also be discussed in this paper.

The deep convection over Central Africa is associated with the year-round world largest lightning activity (Christian et al. 2003). The associated precipitation has unique characteristics compared to other continental regions with, in particular, a relatively small rainfall amount in regard to the amount of high cloudiness (McCollum et al. 2000), or the lightning activity (Takayabu 2006). This is attributed either to the abundance of aerosols, that increases the number of small cloud droplets for the same rain amount, or to a relatively dry boundary layer that elevates the cloud base and decreases the amount of rain reaching the ground. Using Tropical Rainfall Measuring Mission (TRMM) infrared and radar measurements, Liu et al. (2007) showed a larger proportion of nonraining clouds associated with stronger convective updrafts over the Congo basin compared to ocean regions. The smaller rainfall rate is attributed partly to the reasons mentioned above, but also to the fact that more intense updrafts increase the size and/or the optical thickness of the anvil but not necessarily the precipitation. These particularities may impact the coupling between synoptic dynamical disturbances and convection and must be taken into account to interpret results obtained from infrared satellite imagery.

There are only a few observations of MCS characteristics (generation, size, duration, etc.) over Central Africa. Laing and Fritsch (1993) studied MCSs for two years and found west-southwestward propagating systems over Central Africa. Over such a large continental region, the orography (Congo basin and Rift Valley highlands, Fig.1) and surface processes also play an important role in the diurnal initiation of convective systems. Understanding, or at least describing, the interaction between synoptic wave perturbations and the convection must thus take into account the diurnal and propagation characteristics of the MCSs.

The interaction between the continental surface and the atmosphere is also a possible source of intensification for synoptic wave perturbations. Performing a sensitivity test in a Global Circulation Model (GCM), Taylor and Clark (2001) showed that the amplitude of AEWs may be modified by the nature of the soil. In their model, AEWs were amplified because of a larger low-level temperature perturbation. They noted that surface heat and moisture fluxes influence the build-up of convective instability ahead of the wave trough and then the nature of the wave-surface-convection coupling. For Kelvin-like waves on the equator, we may thus also expect a different nature of this coupling that may produce stronger perturbations over continental regions compared to oceanic regions.

The objective of this study is first to describe the nature of the synoptic perturbations of the convection over equatorial Africa and surrounding regions for the different seasons. The remaining part of the study focuses primarily on the boreal spring (March to May) for which the synoptic activity is the strongest. For this season, we analyze the physical source of this variability by inspecting the associated perturbation of (i) the tropospheric dynamics and thermodynamics and (ii) the characteristics of the MCSs embedded in the synoptic dynamical perturbation.

## 2. Data and analysis approaches

### *2.1. Data*

Daily mean OLR data with a spatial resolution of 2.5° (Liebmann and Smith 1996) are used as a proxy for convective activity. The ECMWF ERA-40 reanalyses (Simmons and Gibson 2000) are used to analyze thermodynamic and dynamic perturbations. These data are considered for the 1979-2002 period. As shown in Majda et al. (2004), a previous version of the ECMWF re-analyses (ERA-15) gave smaller wave perturbations compared to radiosondes (a factor of 2 for temperature) over the Pacific Ocean, while the perturbation pattern is preserved. Since there are very few radiosondes in the vicinity of Central Africa, it is possible that wave perturbations of the various atmospheric parameters in ERA-40 analyses are also weak.

Satellite infrared brightness temperatures from the Cloud Archive User Service (CLAUS, Hodges et al. 2000) are also used to detect the convective cloudiness at higher spatiotemporal resolution (0.5°x0.5°, 3 hours). This dataset covers the period from July 1983 to present. It is built from multiple geostationary and polar orbiting satellite imagery in the infrared window channel. The 1984-2002 period is considered in this study. The CPC Merged Analysis of Precipitation (CMAP; Xie and Arkin 1997) data are also used for the period 1979-2002.

### 2.2. *Spectral analysis*

Spectral analyses are based on a simple spectral Fourier analysis of the OLR daily time-series. First, long time-scales (mainly seasonal variation) are removed using a high-pass filter applied to the whole time series (harmonics 1 to 213 corresponding to periods longer than 45 days are removed from the 9617 day time series.). Next, since the synoptic 2-10 day variability of convection is very intermittent with a marked seasonal variation, a power spectrum is computed every 5 days for running time windows of 30 days. This approach makes it possible to define the time evolution of the spectral variance and to compute more reliable monthly mean spectra. A Welch window is applied to the 30-day time series prior to the computation of the spectrum in order to emphasize the central part of the windowed signal and to reduce end effects. The effect of the Welch window on the spectral variance is compensated a posteriori by multiplying the result by the ratio between the total variance of the raw time series and the total variance of the windowed time series.

### 2.3. *Composite methodology*

The composite is based on a time series $OLR_f$, which is the OLR time series first averaged over the Congo basin (15°E-25°E, 5°S-5°N) and then filtered in the 2-10 day band. Oscillations in $OLR_f$ define the different phases (or category) of the quasi-periodic synoptic oscillation of the convection over the Congo basin. The convective development period (between a maximum and a minimum $OLR_f$) is divided in four equal durations, each representing half of a full category (C1, C2, C2, C3). Similarly, the convective dissipation period (between a minimum and a maximum $OLR_f$) is also divided in four parts (C3, C4, C4, C1). Category 1 corresponds to suppressed convection, Category 3 to maximum convection, and categories 2 and 4 correspond respectively to rising and decaying convection. In order to eliminate small or irrelevant oscillations related only to the filtering, we select oscillations having: (i) a duration of between 3 and 7 days and; (b) maximum (and minimum) values larger (smaller) than one standard deviation of the whole filtered time series. Since we want to study specifically the periodic perturbations, we also reject single oscillations (i.e. we only consider series with at least two consecutive oscillations) although this does not affect the results. This approach aims to retain only strong and quasi-periodic convective perturbations over the Congo basin, with no a priori information on the spatial pattern (wave number, direction of propagation, etc.). Using this approach, 114 oscillations are retained for the Congo basin and used to build the composite for March-April 1979-2002. Composites of OLR and ERA-40 data are computed for each 2.5° grid point by averaging the raw (i.e. not time-filtered) time series values in the 4 categories defined above. A Student T-test between pairs of opposite categories (i.e. between category 1-3 and 2-4) is applied to ERA40 parameters for each grid point. In the following, only 99% significant values are presented for wind perturbations. For other parameters, we verified that the T-test is passed for most regions of large amplitudes but all values are presented in order to improve the readability of the figures.

### *2.4. MCS detection and analysis*

A threshold of 233 K in the infrared (~11μm) equivalent brightness temperature is chosen to identify the high cloudiness associated with deep convection. For African and equatorial Atlantic regions, a threshold of 233 K effectively separates the highest cloudiness that peaks after sunset from the mid-level cloudiness that peaks before sunrise (Duvel 1989). For CLAUS images, a pixel is a region of 0.5° x 0.5°. A MCS is defined as an area with continuous pixels colder than 233 K. The size of the MCS is expressed by an effective radius computed assuming a circular shape (Machado et al. 1993). The location of the MCS is defined by its center of mass computed by averaging locations of the various pixels weighted by the difference 233-Tb, where Tb is the brightness temperature of the pixel (Tb $\leq$ 233K by definition). This information is used to analyze the diurnal and the wave modulation of the sizes of the MCSs over different regions. The threshold of 233 K is also used to define a cloud index:

$$CI = \max(0, 233 - Tb)$$

For average maps or composites, this cloud index characterizes high cloudiness without the ambiguities induced by the infrared signature of variations in surface temperature.

Some large MCSs can be followed from one image to another, even for images three hours apart. Such tracking is done here for MCSs (same threshold at 233K) having an effective radius larger than 100 km for more than 6 hours (i.e. present on at least 3 consecutive images.) We perform an automatic tracking of the MCSs, as in William and Houze (1987) and Machado et al. (1998), based on the overlap between two MCSs on two consecutive images. This overlap must be at least 15% of the size of the smallest MCS. If several MCSs cover part of the MCS of the previous image, only the MCS with the largest overlap is considered. Because of the coarse time step, only a simple technique can be used here with no consideration of splitting or merging of identifiable MCSs. The tracking will be used mostly to construct a statistic on MCS propagation speeds.

## 3. The synoptic variability

Between 10°E and 30°E, the minimum OLR value (i.e. the heart of the ITCZ) oscillates seasonally between 10°S in December-January-February (DJF) and 5°N in June-July-August (JJA) (Fig.2). Over the Congo basin, the ITCZ is centered on the equator around April and October and the synoptic variance is larger from November to April. There is a secondary maximum near the coast over the Gulf of Guinea. This synoptic variance remains maximal on the equator for all these months, even if the convection clearly peaks southward between November and February. This suggests that coupled equatorial waves may have an important impact on the synoptic variability.

West of our region of interest, the ITCZ is always located north of the equator with a large synoptic variance from April to August over West Africa and from September to January over the North Equatorial Atlantic Ocean. During JJA over West Africa, the strong synoptic variance between 10°N and 20°N corresponds to the sum of AEWs and Kelvin (Mounier et al. 2007) perturbations with a total variance similar to the variance for the Congo basin in March and April.

Based on these results, the spectral characteristics of the OLR signal are further studied over the Congo basin (15°E-25°E, 5°S-5°N). This is the region of maximum annual mean 2- to 10-day OLR variance (Fig.1). The power spectrum for this region (Fig.3) exhibits a strong peak that clearly denotes synoptic activity dominated by quasi-periodic perturbations of convection. The strongest oscillations (5-6 days) of convective activity are observed when the ITCZ migrates northward over the region in March-April (Fig.3). For this season, the ITCZ is also more active and closer to the equator over the Atlantic (Fig.2). The convective activity breaks off abruptly in June when the ITCZ is the weakest at the equator (Fig.2). This convective activity then progressively recovers as the ITCZ migrates southward over the region between September and November. During this second rainy season, synoptic activity is far weaker and varies on time-scales between 3 to 4 days in September and around 6 days in November.

There are some differences between the two rainy seasons that may partly explain the weaker synoptic activity in October. First, despite similar OLR values, the mean rainfall is larger in October compared to March-April (Fig.3a). This suggests that the discrepancy between convective cloudiness and precipitation (see Introduction) is larger during March-April. Since this large convective cloudiness in regard to rainfall is possibly related to strong convective updrafts, it could also have an impact on the growth of wave perturbations, as demonstrated by Taylor and Clark (2001) for the AEWs. Second, for the March-April season, the ITCZ is closest to the equator from South America to Africa, favoring the initiation of convectively coupled waves over both regions. This also favors the propagation of waves over the equatorial Atlantic. By comparison, the ITCZ is not active in the Gulf of Guinea in October and convection is confined over Central Africa.

Over the Amazon basin (60°W – 70°W), the variance in the 5-6 day band is smaller than for Central Africa and corresponds to a weak peak in the spectrum (Fig. 4c). In addition, this peak occurs mostly toward the end of March, compared to a longer episode between March and May for Central Africa (Fig. 3). Over the West Atlantic (40°W – 50°W), the OLR spectrum shows no peak between 5 and 6 days in March and April (Fig.4b). A better correspondence with the spectrum of Central Africa is obtained for the Gulf of Guinea (0 – 10°E), but the peak at 5 to 6 days also occurs mainly in March (Fig. 4a). For these three regions, the ITCZ is located very close to the equator in March and April and the lack of a periodic activity comparable to this of Central Africa strongly suggest that most of the periodic signal observed here is of local origin. Again, this does not exclude the possibility that convective events over Central Africa might be triggered by perturbations due to Kelvin-type waves coming from the west, with variable impact for different years and seasons. This cannot however explain the robust periodic behavior observed over Central Africa in March and April. Indeed, there is at present no evident physical argument explaining why the Amazon, rather than Central Africa or another equatorial convective region, should be a preferred region for a periodic initiation of Kelvin waves with a period of 5-6 days.

## 4. Composite analysis

A Kelvin wave structure is clearly evident in composite maps of surface pressure and 850 hPa wind perturbations (Fig.5). This is quite remarkable since the composite is obtained by using only the date of the categories (see section 2.3), without any Kelvin space-time filter. The same simple technique does not extract such a well-defined structure if applied to the Amazon region in March-April or to the Pacific region at 7.5°N-172.5°E (i.e. the region studied in Straub and Kiladis 2003) in June-August (not shown). Over Central Africa, these perturbations are centered on the equator and meridional wind anomalies are small. The low-level zonal wind anomaly is in phase with the surface pressure anomaly (i.e. easterly wind for low surface pressure) for the four categories. This is especially evident for category 2 that immediately precedes the minimum OLR over the Congo basin. The OLR is minimal west of the low and east of the high surface pressure anomaly, in a phase that should correspond to maximum convergence for a shallow-water Kelvin wave. This is physically consistent since a maximum in convective activity is associated with stronger low-level convergence. Around Central Africa, the wavelength is around 50° and corresponds to an equivalent depth of 14 m (propagation speed of around 12 $ms^{-1}$) for a Kelvin wave with a period of 5-6 days.

Considering the perturbation in the lower troposphere (Fig.5), the basic physical properties of the Kelvin wave seem to be reproduced, especially the phase quadrature between divergence and surface pressure and the associated eastward propagation. However, there are also some discrepancies with the shallow-water horizontal Kelvin wave pattern. These discrepancies are related partly to the topography of the region. In particular, there is a clear weakening and a latitudinal expansion of the convective anomaly as the disturbance moves over the Rift Valley highlands in category 4. This is also noticeable for the surface pressure anomaly in category 1.

The contrast between the Gulf of Guinea and the Congo basin also gives some regional characteristics, such as the weaker but more persistent OLR anomaly around 10°E (spreading over categories 2 and 3) compared to 20°E (only for category 3). Thus, the wave structure varies as the disturbance propagates eastward from the Gulf of Guinea to the Rift Valley highlands. Other discrepancies are related to the baroclinic structure of the observed perturbation shown in Fig. 6. In particular, the westerly wind anomaly is shifted to the east of the high surface pressure anomaly at 850 hPa (shown in fig. 5) but would be more in phase at 700hPa.

Due to the small number of in situ observations used in the analyses over this region, surface and boundary layer perturbations are mostly due to the parameterization of the ECMWF model. It nevertheless gives a good indication of the potential impact of diabatic processes on the perturbation of temperature and moisture by synoptic disturbances. First, over the continent, the temperature perturbation at low levels is positive east of the OLR minimum (Fig. 6). Because the mid troposphere has a weak temperature modulation, the longitudinal variation of the low level temperature gives enhanced convective instability (larger CAPE) to the east, as shown also for equatorial Pacific regions by Straub and Kiladis (2002, 2003). This may favor the eastward propagation of the convective disturbance. Second, the eastward tilt of the wind perturbation extends down to the surface (first layer on Fig. 6), giving a low-level convergence east of the convection maximum that also favors (or is the signature of) the development of convection to the east and thus the eastward propagation of the convective perturbation.

Temperature and moisture perturbations over Central Africa are largest near the surface (i.e. in the boundary layer), in contrast with the oceanic region of the Gulf of Guinea (Fig. 6). For other ocean regions considered in previous studies (Wheeler et al. 2000, Straub and Kiladis 2003), the temperature perturbation is not maximal at the surface but rather around 700hPa. Indeed, compared to the ocean mixed layer, the soil is expected to have a smaller equivalent specific heat meaning that the surface temperature will be more sensitive to perturbations of the surface fluxes. This gives in particular a larger warming by the increased solar flux during subsiding phase prior to the main convective event. For the Congo basin, ERA-40 gives wave modulation of the incident surface solar flux two (four) times larger than the wave modulation of the latent heat flux (infrared and sensible heat fluxes) (not shown). The cool boundary layer to the west of the convective perturbation (e.g. evaporation of rain) and the warm boundary layer to the east (e.g. enhanced solar radiation at the surface) will amplify the surface pressure gradient. This suggests that the diabatic processes in the boundary layer may increase the amplitude of the wave perturbation. This analysis is not developed further since the physical source and the amplitude of the thermodynamic perturbations reported in figures 5 and 6 may be too model-dependent in ERA-40.

At mid-levels, the large perturbation of upward motion between roughly 400 and 700 hPa is associated with very small temperature perturbations. This suggests that convective warming and adiabatic cooling compensate each other at these pressure levels, maintaining a state of near balance. The net local warming resulting from the ensemble of convective processes (i.e. updraft, downdraft, subsidence in the environment and the various entrainment and detrainment) is thus nearly compensated by vertical motions at the synoptic scale. At high levels, wind and temperature patterns above 300hPa are consistent with a Kelvin or internal gravity wave (e.g. Holton 1992) forced from below by the convective perturbation.

Despite a similar general structure of the wave perturbations, there are some differences compared to results obtained over the Indian Ocean (Wheeler et al. 2000) and the Pacific Ocean (Straub and Kiladis 2003). The moisture perturbation is the largest near the surface and its phase relative to the convective perturbation is different. Over the Pacific, the analysis of Straub and Kiladis (2003) shows that the moisture is maximal east of the convection maximum, but for Central Africa, the moisture perturbation at low level is positive slightly west of the OLR minimum (Fig. 6). This may be attributed again to the difference between marine and continental boundary layers. Over the ocean, convection tends to cool and dry the boundary layer (small variation of the relative humidity), while over continental regions, one may expect a moistening due to the evaporation of rain, even in a cooler environment.

## 5. Convective systems

### *5.1.* *A case study*

In March and April 1997, there is a very clear quasi-periodic modulation of the convective activity over Central Africa (Fig. 7a). For this period, the phenomenon unambiguously dominates the synoptic variability over Central Africa. A notable point is the variable propagation speed of the convective cloud anomaly from one event to another. There is in particular a relatively slow eastward propagation (9-10ms$^{-1}$) between 24 and 29 March (Fig.7, line A), but there are also convective events without clear propagation on March 17 (Fig.7, line B) or April 12. The longitudinal extension of the convective perturbation is also variable. Some convective events propagate from 15°W to 40°E (Fig.7, line A) but other events are confined between 10°E and 35°E (Fig. 7, line B). These later events thus propagate over half of the average wavelength (50°) deduced from the composite. Between 15 and 24 March, the first two convective events are also associated with weak local westerly wind anomalies. With a better spatio-temporal resolution (Fig. 7b), the signature of individual MCSs is discernible. As already reported in Laing and Fritsch (1993), these MCSs tend to move westward over Central Africa and the neighboring

Atlantic Ocean. The eastward propagation of the convective perturbation “envelope” is still observable, but as a succession of daily convective events propagating westward. For this time-longitude diagram, most MCSs are observable for one day or so. Occasionally, some MCSs persist for a longer period, such as around April 14, when a MCS lasts for more than 2 days and propagates from 30°E to 10°W along the equator at a zonal speed of around $14 ms^{-1}$ (Fig.7, line C), establishing an interesting link between two oscillations.

For this period, it is hard to see systematic dynamical perturbations coming from the west prior to the convective events such as, for example, low-level wind disturbance that could propagate eastward from the Atlantic and then trigger convection near the coast. Rather, strong westerly wind anomalies appear near the coast in the Gulf of Guinea in April 1997 and indeed follows by one or two days the development of a convective perturbation at 10°E (Fig. 7a). The strong westerly wind anomalies appear while this convective perturbation moves eastward and grows over the Congo Basin in association with westward propagating MCSs (Fig. 7b). As already discussed from the spectral characteristics of the perturbations over region located further west (Fig. 4), this confirms that part of these convective perturbations are likely to be triggered by local processes and not by eastward moving disturbances coming from the Atlantic. Near the end of March, however, two strong convective events are associated with perturbations coming from the Atlantic that disrupt the local periodic oscillation over Central Africa.

### *5.2. Average diurnal variation*

The diurnal response of convection to solar forcing is a robust characteristic of a region that depends mostly on the topography (land-sea contrast, orography) and must be taken into account to better understand the nature of the interaction between synoptic disturbances and convection. There is indeed a strong impact of the topography on both phase and amplitude of the average diurnal variation of the convective cloudiness along the equator (Fig. 8). The convective cloud cover is triggered over highlands located either near the coast (10-15°E) or west of the Rift Valley (25-30°E). The maximum convective activity occurs west of Lake Victoria (i.e. ~27.5°E) between 12 and 18 GMT. Over the Congo basin, the convective cloud cover is smallest between 9 and 12 GMT and largest at 18 GMT, with a weak secondary maximum at 3 GMT. Near the coast at 10°E, convection appears after midnight and persists until 18GMT. An average diurnal westward propagation of the convective cloudiness is also apparent on the western slopes of highlands near 10, 30 and 35°E (note the maximum convection between 3 and 6 GMT over Lake Victoria due to land-lake breeze). This propagation could be related to the westward propagation of MCSs, as in Laing and Fritsch (1993) and Laing et al (2008), but also to cirrus advection by the Tropical Easterly Jet. The average speed that can be deduced from the time-longitude diagram varies between 7 $ms^{-1}$ (Fig. 8, line A) and 4 $ms^{-1}$ (Fig. 8, line B). This is far smaller than the speed of the MCSs observed for March-April 1997 (Fig. 7). This speed is closer to the average easterly wind at 200 hPa that varies between 10 $ms^{-1}$ in March and 6 $ms^{-1}$ in April (Nicholson and Grist 2003).

### *5.3. <u>Diurnal and wave composites</u>*

The aim of this section is to analyze the Kelvin wave modulation of the convective activity taking into account diurnal variations. To build this composite, a reference day and hour must first be selected. This time reference is midnight for the day corresponding to a minimum in the filtered OLR time series. Only strong and persistent oscillations are selected with the criteria already used for the composite analysis above (see section 2). Then, the composite is simply done by averaging the brightness temperature, or the cloud index, for each of the 48 time steps (6 days) located before and after this reference hour. This approach gives a composite view of the synoptic perturbation that preserves the diurnal information (Fig. 9).

The diurnal triggering of the convection related to the orography near 30°E occurs in every phase of the synoptic perturbation. By contrast, there are strong wave modulations of the diurnal cycle over the Congo basin and over the equatorial Atlantic. The westward propagation of the cloud perturbation is clear over the Atlantic, with an apparent phase speed of 14 $ms^{-1}$ (Fig. 9, line A), much larger than the speed (~6 $ms^{-1}$) visible for the average diurnal cycle (Fig. 8, line A) near 10°E. The slower propagation near 10°E is however also visible in figure 9. One possible interpretation is that the apparent propagation over the Atlantic is actually due to MCSs while the slower propagation near 10°E could be related to local (land-sea breeze, orography) effects or simply to cirrus advection by the upper tropospheric jet. Over the Congo basin, there is no obvious propagation of the cloud signal. This suggests that long-lived MCSs propagating westward in figure 7 have no systematic phase locking with respect to the synoptic wave perturbation.

### 5.4. Size, speed and duration of the MCS

Three classes of size are defined corresponding to an equivalent radius less than 200 km, between 200 and 500 km and greater than 500 km. The wave modulation of the convective cloud cover increases with the MCS size (Fig.10). The cloud cover due to small MCSs (Fig.10a) is a maximum over the highlands around 30°E and near the coast. For these small MCSs, the diurnal variation clearly dominates over the wave modulation and there is no clear propagation of the cloud signal. For the intermediate size class (Fig.10b), the cloud cover is the largest west of the Rift Valley highlands. There is a relatively strong wave modulation of the cloud cover between 10°E and 35°E that closely follows the eastward propagation of the negative OLR anomaly. Westward propagating elements in the cloud signal are also detectable but with various phase speeds between 12 $ms^{-1}$ (Fig. 10, line B) and 20 $ms^{-1}$ (Fig. 10, line A) depending on the case considered, suggesting that these apparent propagation characteristics could be due to sampling effects. The largest MCSs (Fig. 10c), are confined over the Congo basin and appear only in wave categories corresponding to the maximum convective activity. The amplitude of wave modulation of the convective cloud cover for these large MCSs is three times larger than for the smaller classes of size. The maximum wave modulation of the convective cloud cover found over the Congo basin (Figs 2 and 3) is thus mostly due to these large MCSs. This means that the 5-6 day synoptic variability over Central Africa is related mostly to the growth of these large MCSs and not so much to the local diurnal triggering of convective systems. These large MCSs in category 3 may be associated with the large updrafts found over Central Africa in previous studies (Liu et al. 1987).

As mentioned in section 2, tracking techniques may be used to obtain some characteristics of the MCS life cycle and their interaction with the wave synoptic perturbation. We report these characteristics only for MCSs having a center of mass in the Congo basin region at least once during their life cycle. The computation of the speed of these MCSs is not straightforward. In particular, MCSs merging with other MCSs or splitting into a few MCSs will occasionally result in "jumps" of the center of mass and thus in false estimate of the MCS speed between two time steps. In order to minimize the impact of these jumps, only the average speed between the first and last positions of the MCSs is considered. The zonal speed distribution (Fig. 11) clearly exhibits a preference for westward motion with a maximum occurrence around -12 $ms^{-1}$. The meridional speed distribution shows a preference for southward motion of MCSs with a maximum occurrence around -4 $ms^{-1}$. This result confirms that most MCSs have a west-southwestward propagation over Central Africa, consistent with results of Laing and Fritsch

(1993) for a few cases in 1986-87. In a more recent paper, Laing et al. (2008) confirm this result and also showed that MCSs tend to be initiated in the lee side of high terrain over Africa, consistent with thermal forcing from elevated heat sources, as also visible in Figs. 8 and 9.

The distribution of the duration of these systems (Fig. 11) shows a most probable lifetime of 6 hours (i.e. the minimum duration threshold). The MCS occurrence decreases progressively as the duration increases, with only very few MCSs being traceable for more than 3 days. When only MCSs being over the Congo basin during category 3 (minimum OLR) are considered, there are relatively more persistent MCSs with secondary peaks around 21h, 33h and 42h. These secondary peaks can be partly related to the diurnal cycle (systems merging to newly generated ones in the afternoon, dissipation in morning hours, etc.). In particular, a larger amount of MCSs present over the Congo Basin in category 3 dissipates around 13 - 16 LST instead of 04 - 07 LST (not shown). As expected, these MCSs are generally initiated in categories 2 or 3 and they dissipate in categories 3 or 4 (Fig. 12). More interestingly, due to the dominant west-southwestward propagation of the MCSs, long duration MCSs are preferentially initiated east-northeast of the Congo basin in categories 2, i.e. when the maximum convection is actually located between the Greenwich meridian and 10°E (Fig. 5). Between 25°E and 30°E, there is indeed a weak modulation of the MCS initiation by the wave (Fig. 10a), and those initiated in category 2 (i.e. the category just before the maximum convection over the Congo basin) are more persistent (Fig. 11). Most of these persistent MCSs will dissipate west-southwest of the Congo basin in category 4 (Fig. 12), when suppressed conditions dominate at the synoptic scale (Fig. 5). Note that some less persistent MCSs initiate and dissipate over the Congo basin in category 3. Debatable configurations are also visible, such as persistent MCSs dissipating around 32.5°E in category 4 after being present over the Congo basin in category 3. This is due partly to some drawbacks of the tracking technique. The general behavior of the MCSs relative to the synoptic perturbation is nevertheless well depicted by this tracking technique.

## 6. Summary and discussion

Spectral and composite analyses of the OLR signal reveal strong and reproducible 5-6 day oscillations of the convective activity that dominate the intraseasonal variability over Central Africa during boreal spring. The eastward propagation of the wave, its wavelength and its associated dynamical structure suggest a Kelvin-like perturbation. Compared to previous similar studies on such coupled equatorial waves, this study focuses on a continental region for which the oscillation dominates the synoptic variability in boreal spring. The well-defined Kelvin-like structure thus appears from a simple composite analysis based only on a filtered OLR signal in the 2-10 day spectral band (it is not necessary to filter more specifically in a predefined Kelvin space-time spectral domain). In addition, this study reveals that the synoptic perturbation of the convection over the Congo basin is mostly related to large (Req > 500km), persistent (duration between 15 and 45 hours) MCSs moving west-southwestward from the Rift Valley. These MCSs tend to dissipate near the coast where they encounter suppressed conditions. During the following days, small and medium MCSs (Figs. 10a and 10b) are still generated over the Rift Valley, but they cannot grow over the Congo basin anymore since the convective instability is then smaller. MCSs generated near the coast also move westward but they do not grow, certainly because of the smaller convective instability over the equatorial Atlantic. The Congo basin thus appears as the only region where large systems generated over the Rift Valley can grow while propagating westward, if they encounter favorable conditions (larger conditional instability, low-level moisture convergence). These favorable conditions can be related either to Kelvin-type waves coming from the Atlantic or to local processes. While this deserves further investigation, based in particular on numerical experiments, the origin of these perturbations is further discussed in the following.

For Kelvin waves propagating over the equatorial Atlantic, the observed growth of the convective and dynamical disturbances near the coast of Equatorial Africa could be attributed to a larger conditional convective instability that enhances locally the amplitude of the perturbation. Also, the larger perturbation of the low-level temperature over continental region may favor the wave growth. Such an effect has already been demonstrated for AEW (Taylor and Clark 2001) and deserves further investigation for the 5-6 day oscillation. As discussed above, the maximum amplitude of the perturbation over the Congo basin can be attributed to the growth of the convective systems encountering favorable conditions in wave category 3 while they propagate westward from the Rift Valley. However, despite the equatorial position of the ITCZ, the robust 5-6 day peak does not appear over the west equatorial Atlantic in March and April. It is thus unlikely that such Kelvin wave trains can explain the robust 5-6 day oscillation.

An alternative is that the oscillation is related to local processes. We can only give some hypotheses at this stage. The oscillation of the convection over the Congo basin could be forced by processes analogous to the "discharge-recharge" or local instability theory (Bladé and Hartmann 1993, Hu and Randal 1994) that drive periodic convective development mainly because of the delay necessary to rebuild the convective instability after a strong convective episode. This is only an analogy since this theory was illustrated using simple models for intraseasonal 40-50 days oscillations of the convection over the ocean with a fixed SST. The coupling between the convection and the surface could have a major impact here. The growth of the convective systems coming from the Rift Valley could be given by the increased convective instability related to the recharge phase. The eastward propagation of the perturbation and the

Kelvin-type wave pattern could be favored by the large positive (negative) surface temperature anomaly east (west) of the maximum convective perturbation over the continent. Without going too far in the framework of the present discussion, it will certainly be an interesting point to consider also the difference in the dominant period of the oscillation with 3-4 days in August-September and 5-6 days in March-April (Fig. 3) in regard to this local instability theory associated with seasonal changes in the mean large scale circulation and in the surface characteristics. Such studies are needed for a better knowledge of the origin of these oscillations and could also be important to improve current weather forecasts over Central Africa or other tropical regions.

**Acknowledgements**: We would like to thank George Kiladis, Chris Thorncroft, Daniel Nethery and Prince Xavier for useful discussions and helpful comments on the manuscript.

## References


Bladé, I., and D.L. Hartmann, 1993: Tropical Intraseasonal Oscillations in a Simple Nonlinear Model. *J. Atmos. Sci.*, **50**, 2922–2939.

Christian H. J., Coauthors, 2003: Global frequency and distribution of lightning as observed from space by the Optical Transient Detector. *J. Geophys. Res.*, **108**, 4005, doi:10.1029/2002JD002347.

Diedhiou A., S. Janicot, and A. Viltard, 1999: Easterly wave regimes and associated convection over West Africa and tropical Atlantic ocean: Results from NCEP/NCAR and ECMWF reanalysis. *Climate Dyn.*, **11**, 795–822.

Duvel, J.P., 1989: Convection over Tropical Africa and the Atlantic Ocean during Northern Summer. Part I: Interannual and Diurnal Variations. *Mon. Wea. Rev.*, **117**, 2782–2799.

Duvel J. P., 1990: Convection over tropical Africa and the Atlantic Ocean during northern summer. Part II: Modulation by easterly waves. *Mon. Wea. Rev.*, **118**, 1855–1868.

Fink A. H., and A. Reiner, 2003: Spatio-temporal variability of the relation between African Easterly Waves and West African Squall Lines in 1998 and 1999. *J. Geophys. Res.*, **108**, 4332, doi:10.1029/2002JD002816.

Hodges, K.I., D.W. Chappell, G.J. Robinson, and G. Yang, 2000: An Improved Algorithm for Generating Global Window Brightness Temperatures from Multiple Satellite Infrared Imagery. *J. Atmos. Oceanic Technol.*, **17**, 1296–1312.

Holton J. R., 1992: *An Introduction to Dynamic Meteorology*. 3d ed. Academic Press, 511 pp.

Hu, Q., and D.A. Randall, 1994: Low-Frequency Oscillations in Radiative-Convective

Systems. *J. Atmos. Sci.*, **51**, 1089–1099

Kiladis G. N., C. D. Thorncroft, and N. G. Hall, 2006: Three-dimensional structure and dynamics of African easterly waves. Part I: Observations. *J. Atmos. Sci.*, **63**, 2212–2230.

Laing, A.G., and J.M. Fritsch, 1993: Mesoscale Convective Complexes in Africa. *Mon. Wea. Rev.*, **121**, 2254–2263.

Laing, A.G., R. Carbone, V. Levizzani, and J. Tuttle, 2008: The propagation and diurnal cycles of deep convection in northern tropical Africa. *Quart. J. Roy. Meteor. Soc.*, **134**, 93–109.

Liebmann, B., G. N. Kiladis, L. M. V. Carvalho, C. Jones, C. S. Vera, I. Bladé, and D. Allured, 2008: Origin of convectively coupled Kelvin waves over South America. *J. Climate* (accepted).

Liu, C., E.J. Zipser, and S.W. Nesbitt, 2007: Global Distribution of Tropical Deep Convection: Different Perspectives from TRMM Infrared and Radar Data. *J. Climate*, **20**, 489–503

McCollum, J. R., A. Gruber, and M. B. Ba, Discrepancy between gauges and satellite estimates of rainfall in equatorial Africa, J. Appl. Meteorol., 39, 666– 679, 2000.

Machado L. A. T., J.-P. Duvel, and M. Desbois, 1993: Diurnal variations and modulation by easterly waves of the size distribution of convective cloud clusters over West Africa and the Atlantic Ocean. *Mon. Wea. Rev.*, **121**, 37–49.

Machado, L.A.T., W.B. Rossow, R.L. Guedes, and A.W. Walker, 1998: Life Cycle Variations of Mesoscale Convective Systems over the Americas. *Mon. Wea. Rev.*, **126**, 1630–1654.

Majda, A.J., B. Khouider, G.N. Kiladis, K.H. Straub, and M.G. Shefter, 2004: A Model for Convectively Coupled Tropical Waves: Nonlinearity, Rotation, and Comparison with

Observations. *J. Atmos. Sci.*, **61**, 2188–2205.

Mekonnen, A., C.D. Thorncroft, and A.R. Aiyyer, 2006: Analysis of Convection and Its Association with African Easterly Waves. *J. Climate*, **19**, 5405–5421.

Mounier, F., G. N. Kiladis and S. Janicot, 2007: Analysis of the dominant mode of convectively coupled Kelvin waves in the West African monsoon. *J. Climate,* **20**, 1487-1503.

Nicholson, S.E., and J.P. Grist, 2003: The Seasonal Evolution of the Atmospheric Circulation over West Africa and Equatorial Africa. *J. Climate*, **16**, 1013–1030.

Payne S. W., and M. M. McGarry, 1977: The relationship of satellite inferred convective activity to easterly waves over west Africa and the adjacent ocean during Phase III of GATE. *Mon. Wea. Rev.*, **105**, 414–420.

Reed R. J., D. C. Norquist, and E. E. Recker, 1977: The structure and properties of African wave disturbances as observed during Phase III of GATE. *Mon. Wea. Rev.*, **105**, 317–333.

Straub, K.H., and G.N. Kiladis, 2002: Observations of a Convectively Coupled Kelvin Wave in the Eastern Pacific ITCZ. *J. Atmos. Sci.*, **59**, 30–53.

Straub, K.H., and G.N. Kiladis, 2003: The Observed Structure of Convectively Coupled Kelvin Waves: Comparison with Simple Models of Coupled Wave Instability. *J. Atmos. Sci.*, **60**, 1655–1668.

Takayabu, Y. N. (2006), Rain-yield per flash calculated from TRMM PR and LIS data and its relationship to the contribution of tall convective rain, *Geophys. Res. Lett.*, *33*, L18705, doi:10.1029/2006GL027531.

Taylor C., and D. Clark, 2001: The diurnal cycle and African easterly waves: A land surface perspective. *Quart. J. Roy. Meteor. Soc.*, **127**, 845–867.

Wang, H., and R. Fu, 2007: The Influence of Amazon Rainfall on the Atlantic ITCZ through Convectively Coupled Kelvin Waves. *J. Climate*, **20**, 1188–1201.

Wheeler, M., and G.N. Kiladis, 1999: Convectively Coupled Equatorial Waves: Analysis of Clouds and Temperature in the Wavenumber–Frequency Domain. *J. Atmos. Sci.*, **56**, 374–399.

Wheeler, M., G.N. Kiladis, and P.J. Webster, 2000: Large-Scale Dynamical Fields Associated with Convectively Coupled Equatorial Waves. *J. Atmos. Sci.*, **57**, 613–640.

Williams, M., and R.A. Houze, 1987: Satellite-Observed Characteristics of Winter Monsoon Cloud Clusters. *Mon. Wea. Rev.*, **115**, 505–519.

Xie, P., and P.A. Arkin, 1997: Global Precipitation: A 17-Year Monthly Analysis Based on Gauge Observations, Satellite Estimates, and Numerical Model Outputs. *Bull. Amer. Meteor. Soc.*, **78**, 2539–2558

Yang, G.Y., B. Hoskins, and J. Slingo, 2003: Convectively Coupled Equatorial Waves: A New Methodology for Identifying Wave Structures in Observational Data. *J. Atmos. Sci.*, **60**, 1637–1654.

# Figure Captions

Figure 1: (a) Orography (m) and (b) annual average OLR (shadings in W $m^{-2}$) and annual average 2-10 day spectral variance of the OLR (contour in [W $m^{-2}]^2$) for the 1979-2002 period. The box indicates the Congo basin region used in this study.

Figure 2: Monthly average (shadings in W $m^{-2}$) and 2-10 day spectral variance (contours in [W $m^{-2}]^2$) of the OLR for the 1979-2002 period. The squares on the March panel represent regions further analyzed on Fig. 4.

Figure 3: Average seasonal cycle (1979-2002) over the Congo basin (5S-5N, 15E-25E) for : (a) CMAP (solid line) and ERA40 (dashed line) precipitation (mm $d^{-1}$); (b) OLR (solid line, W $m^{-2}$) and 2-10-day spectral variance (dashed line, [W $m^{-2}]^2$ ) and; (c) OLR power spectrum [W $m^{-2}]^2$.

Figure 4: Average seasonal cycle (1979-2002) of the OLR power spectrum for different equatorial regions (5°N-5°S) defined on the March panel of figure 2: (a) Gulf of Guinea (0-10°E), (b) West Atlantic (40°W-50°W) and (c) Amazon basin (60°W-70°W).

Figure 5: Average horizontal structure of the perturbation given by the composite obtained from the 2-10 day filtered OLR signal averaged over the Congo basin in March and April 1979-2002. Shadings represent the OLR anomaly (W $m^{-2}$); vectors represent the ERA-40 850 hPa wind anomaly (reference vector is 1.5 m $s^{-1}$); contours represent the ERA-40 surface pressure anomaly (hPa).

Figure 6: Composite values averaged from 5°S to 5°N: (top panels) OLR anomaly (W $m^{-2}$); (center panels) vertical structure for specific humidity (shadings g $kg^{-1}$) and divergence (contours intervals $10^{-6}$ $s^{-1}$); (bottom panels) temperature (shadings K) and zonal-vertical circulation (vertical velocity in m $s^{-1}$ is amplified 100 times).

Figure 7: Time-longitude diagrams of 5°S – 5°N average in March-April 1997 for: (a) daily OLR (shadings in W $m^{-2}$) and 6-hourly ERA-40 surface zonal wind (contours in m $s^{-1}$) and; (b) 3-hourly cloud index (shadings in K) and 6-hourly ERA-40 surface zonal wind anomaly (contours in m $s^{-1}$).

Figure 8: Time-longitude diurnal composite of the cloud index averaged from 5°S to 5°N for March and April of the 1984-2002 period. The corresponding orography is shown at the bottom of the figure.

Figure 9: Composite time-longitude diagrams of 5°S – 5°N average for March-April 1984-2002 for 3-hourly cloud index (shadings in K) and daily OLR anomalies (contours in W $m^{-2}$). The ordinates origin is midnight for the day corresponding to a minimum in the filtered OLR time series.

Figure 10: As in figure 9 but for the percentage of pixels over the Congo basin covered by MCS with equivalent radius (a) smaller than 200 km, (b) between 200-500 km and (c) greater than 500 km (shadings in %).

Figure 11: (Top) Distribution of average zonal and meridional speed for convective systems having their center of mass over the Congo basin at least once during their existence. (Bottom) Distribution of the duration of these systems, either for all systems or only for those being over the Congo basin in wave category 3.

Figure 12: Wave category (1 to 4) and (top) initial and (bottom) final positions of convective systems having their center of mass over the Congo basin in wave category 3 at least once during their existence. The size of the marker is proportional to the duration of the corresponding convective systems.

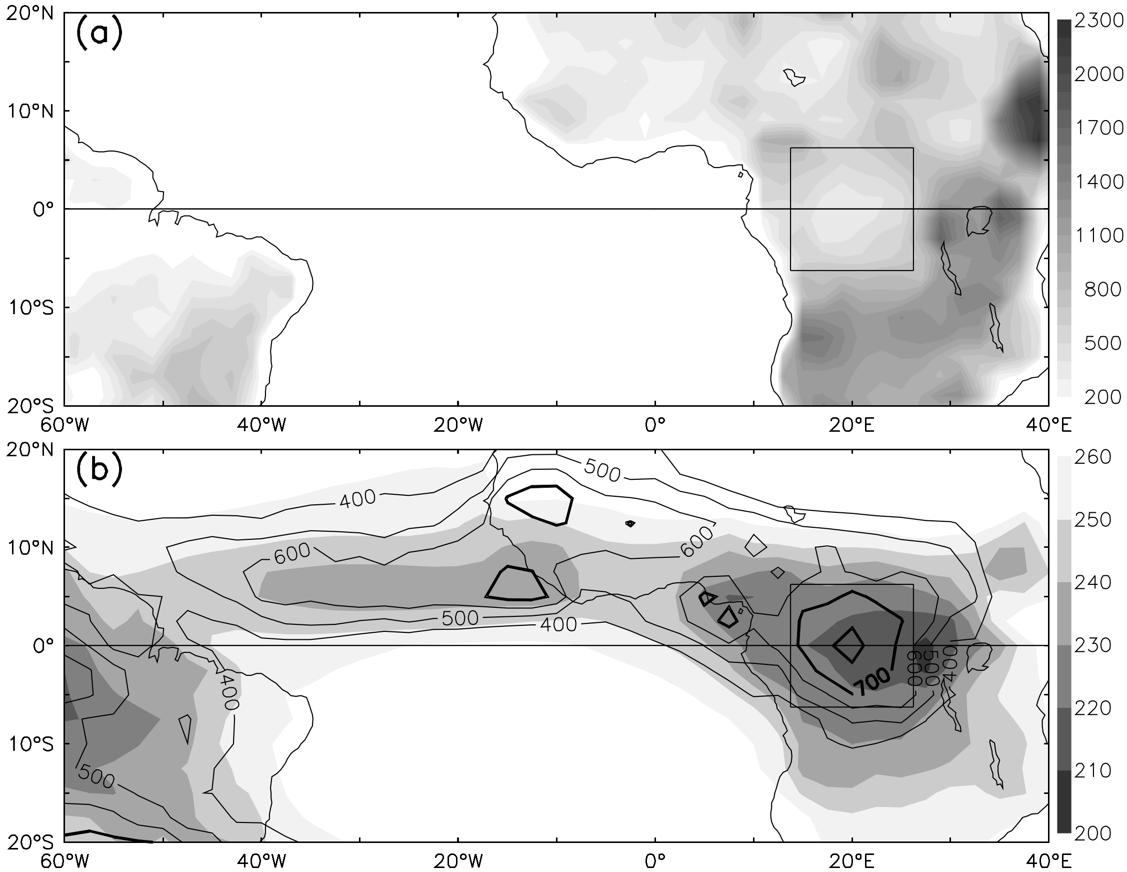


Figure 1: (a) Orography (m) and (b) average OLR (shadings in W m−2) and average 2-10 day spectral variance of the OLR (contour in [W m−2]2) for the 1979-2002 period. The box indicates the Congo basin region used in this study.

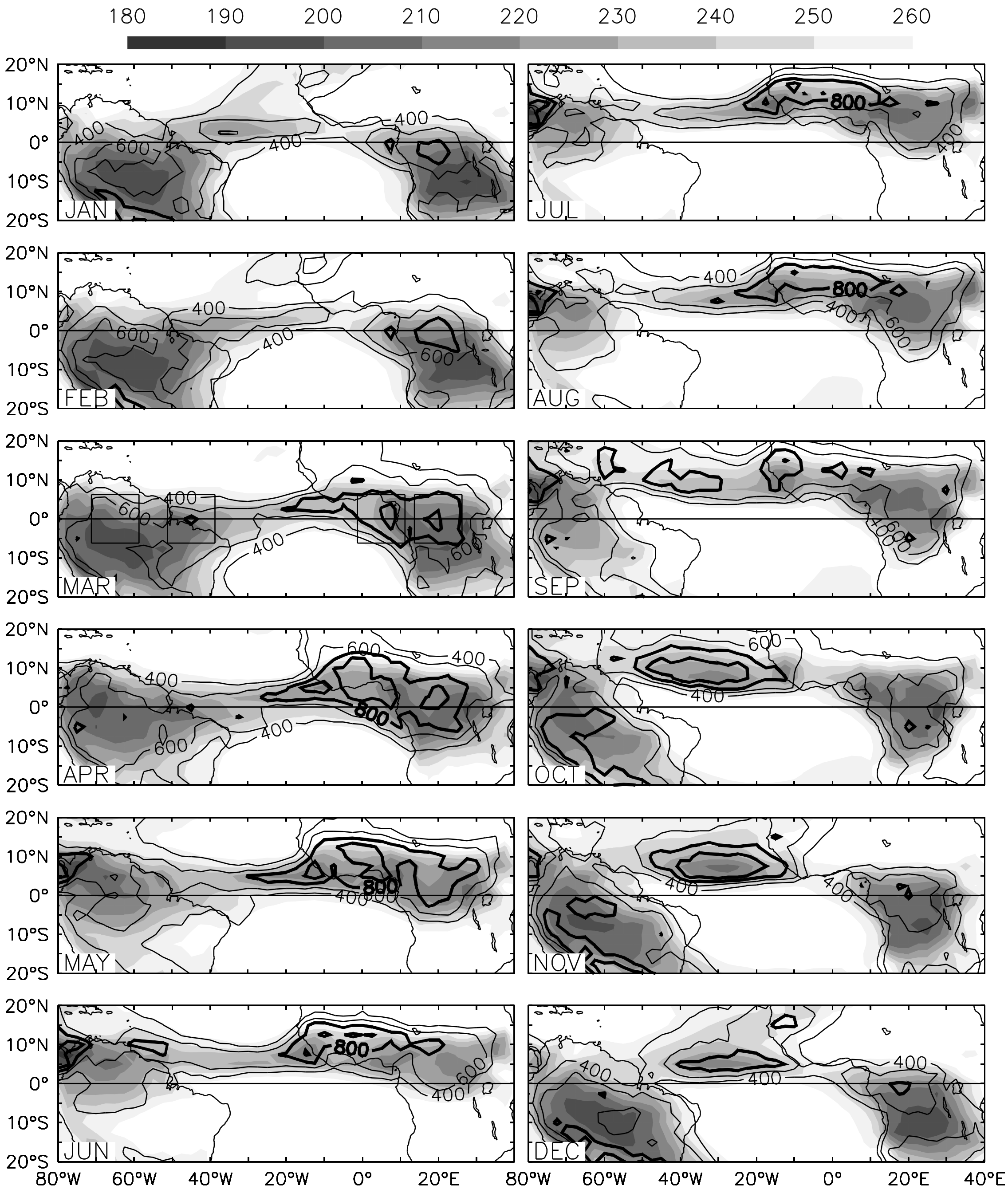


Figure 2: Monthly average (shadings in W m−2) and 2-10 day spectral variance (contours in [W m−2]2) of the OLR for the 1979-2002 period. The squares on the March panel represent regions further analyzed on Fig. 4.

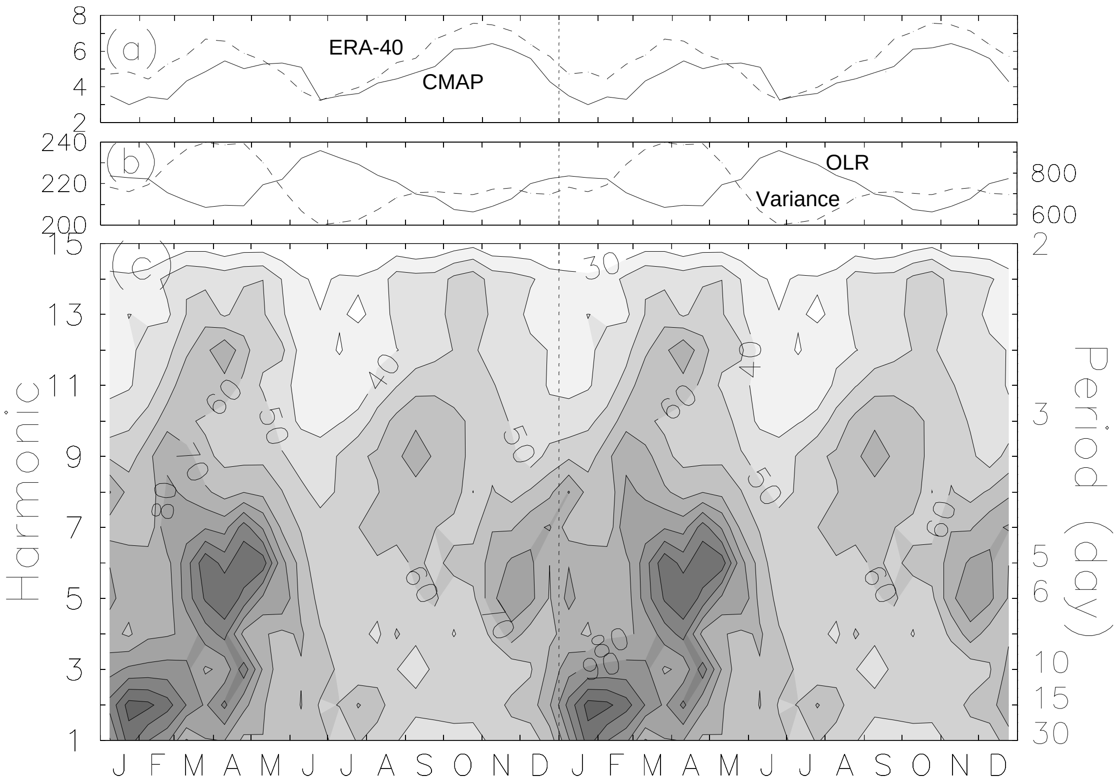


Figure 3: Average seasonal cycle (1979-2002) over the Congo basin (5S-5N, 15E-25E) for : (a) CMAP (solid line) and ERA40 (dashed line) precipitation (mm d-1); (b) OLR (solid line, W m−2) and 2-10-day spectral variance (dashed line, [W m−2]2 ) and; (c) OLR power spectrum [W m−2]2.

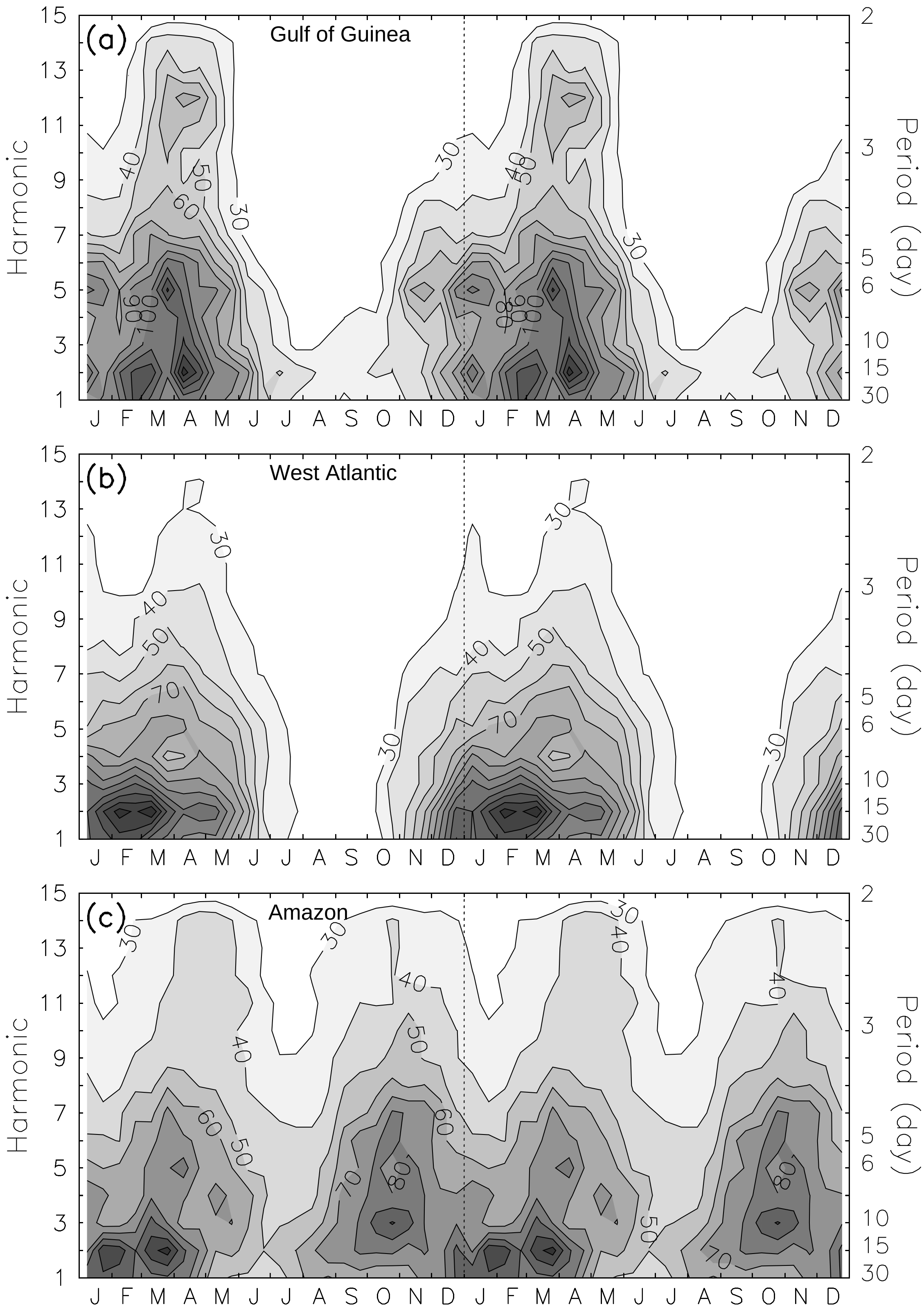


Figure 4: Average seasonal cycle (1979-2002) of the OLR power spectrum for different equatorial regions (5°N-5°S) defined on the March panel of figure 2: (a) Gulf of Guinea (0-10°E), (b) West Atlantic (40°W-50°W) and (c) Amazon basin (60°W-70°W).

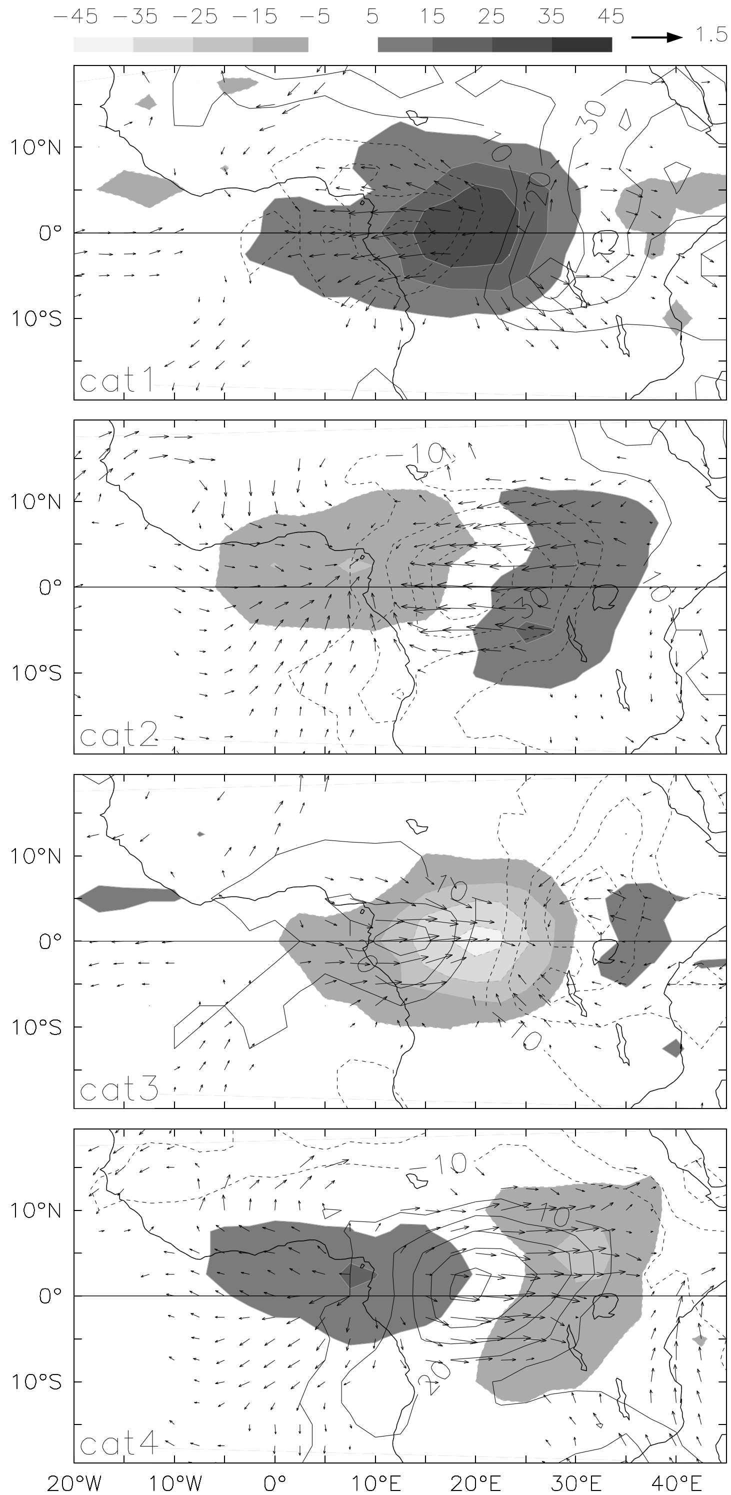


Figure 5: Average horizontal structure of the perturbation given by the composite obtained from the 2-10 day filtered OLR signal averaged over the Congo basin in March and April 1979-2002. Shadings represent the OLR anomaly (W m−2); vectors represent the ERA-40 850 hPa wind anomaly (reference vector is 1.5 m s-1); contours represent the ERA-40 surface pressure anomaly (hPa).

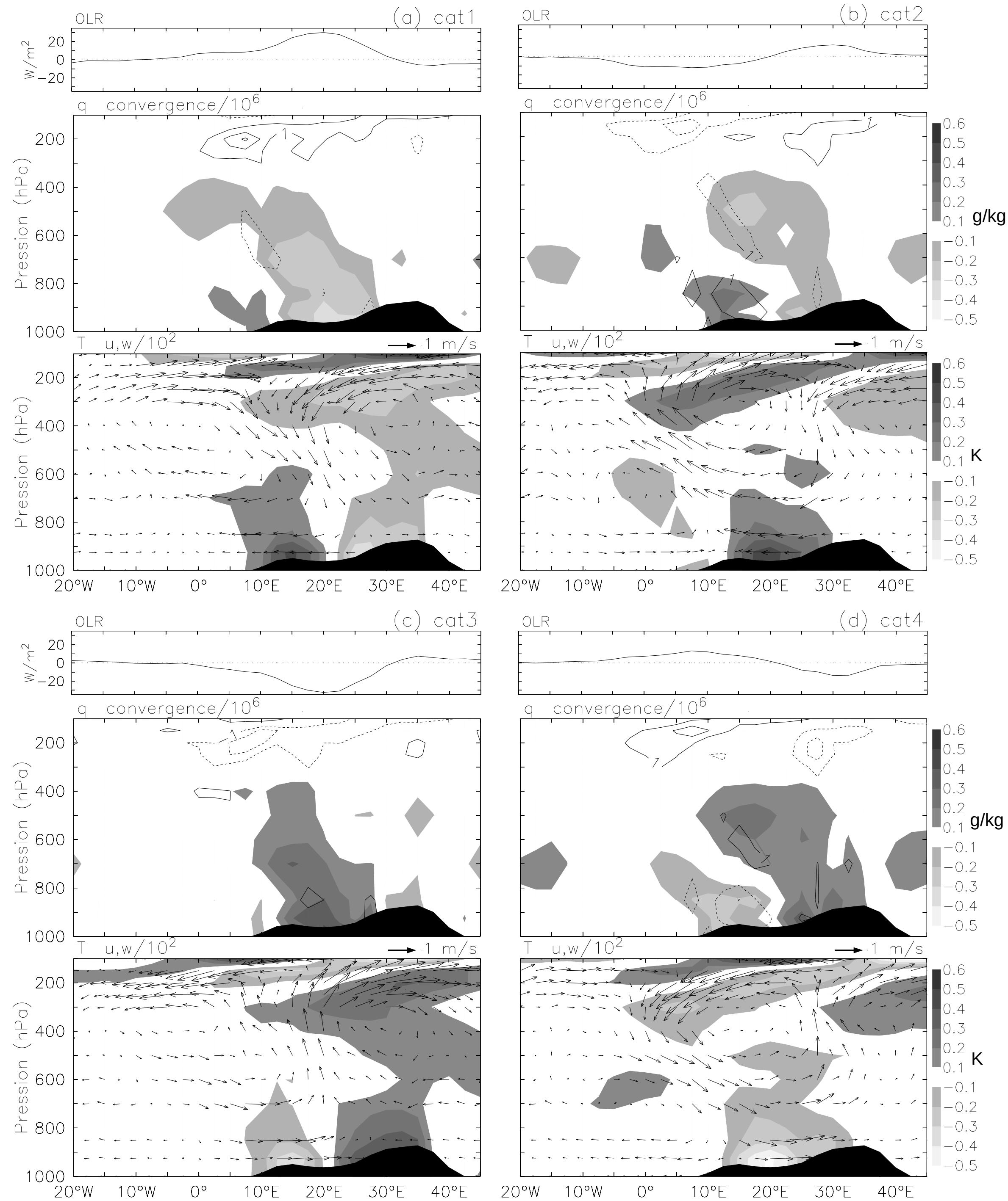


Figure 6: Composite values averaged from 5°S to 5°N: (top panels) OLR anomaly (W m−2); (center panels) vertical structure for specific humidity (shadings g kg-1) and divergence (contours intervals 10−6 s−1); (bottom panels) temperature (shadings K) and zonal-vertical circulation (vertical velocity in m s-1 is amplified 100 times).

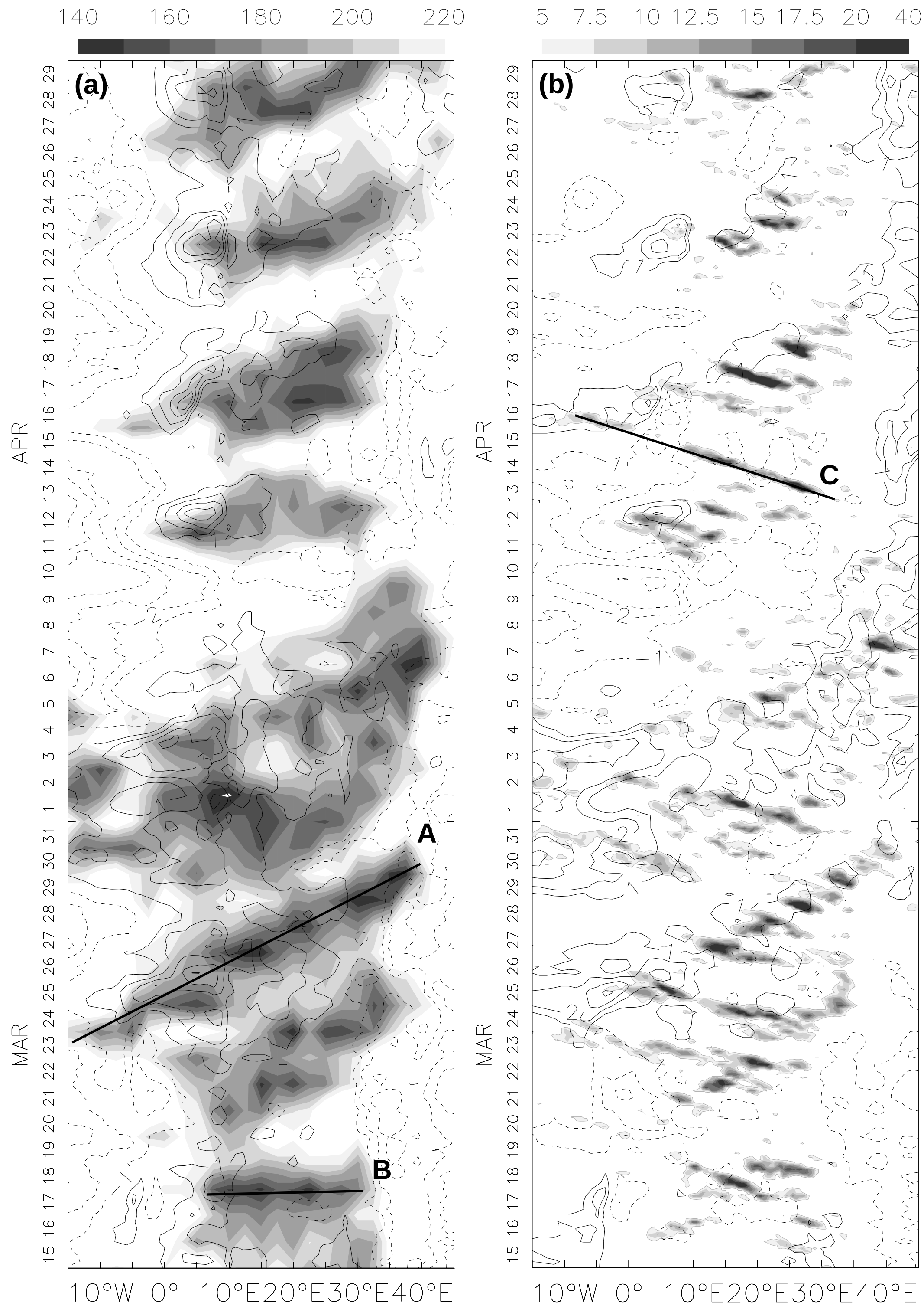


Figure 7: Time-longitude diagrams of 5°S – 5°N average in March-April 1997 for: (a) daily OLR (shadings in W m−2) and 6-hourly ERA-40 surface zonal wind (contours in m s-1) and; (b) 3-hourly cloud index (shadings in K) and 6-hourly ERA-40 surface zonal wind anomaly (contours in m s-1).

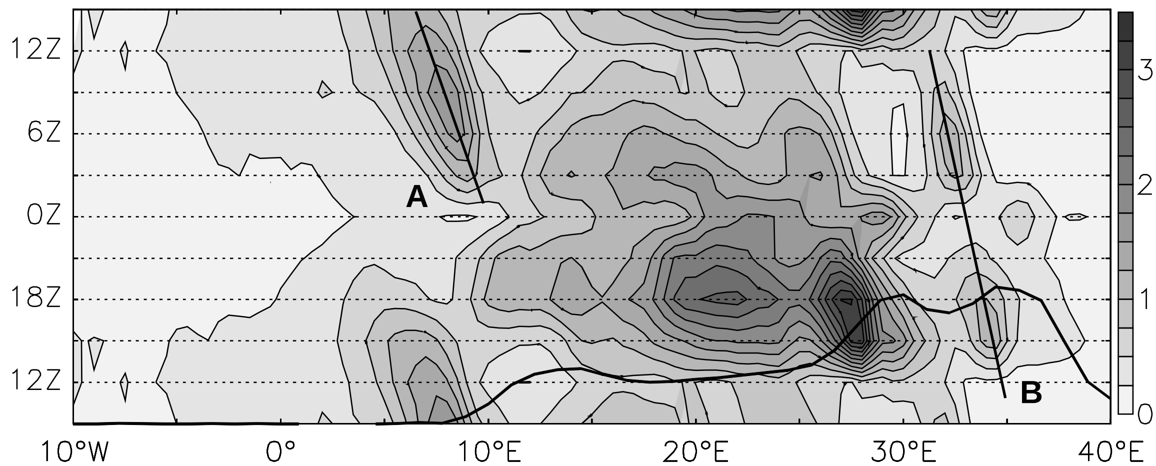


Figure 8: Time-longitude diurnal composite of the cloud index averaged from 5°S to 5°N for March and April of the 1984-2002 period. The corresponding orography is shown at the bottom of the figure.

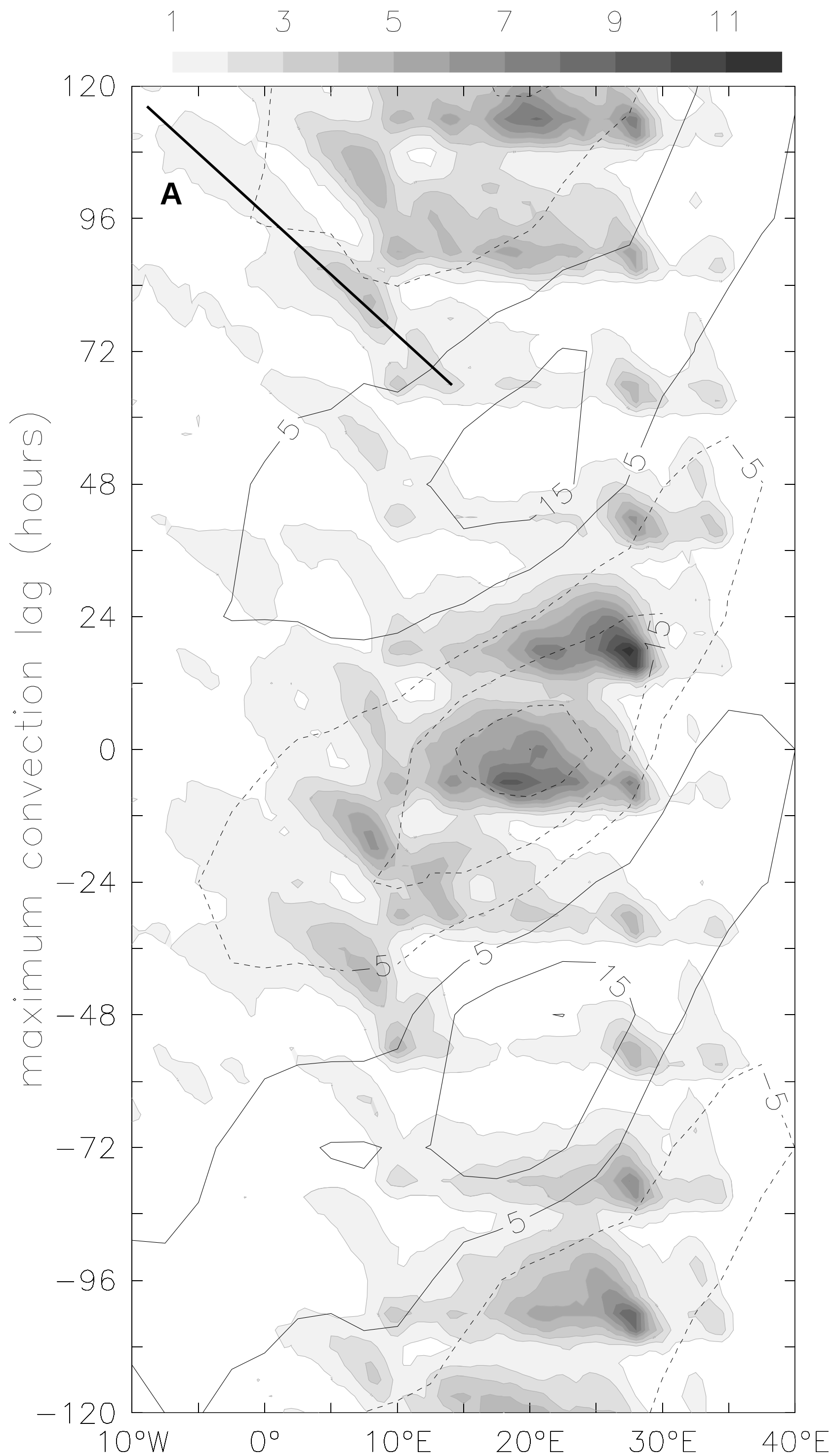


Figure 9: Composite time-longitude diagrams of 5°S – 5°N average for March-April 1984-2002 for 3-hourly cloud index (shadings in K) and daily OLR anomalies (contours in W m2). The ordinates origin is midnight for the day corresponding to a minimum in the filtered OLR time series.

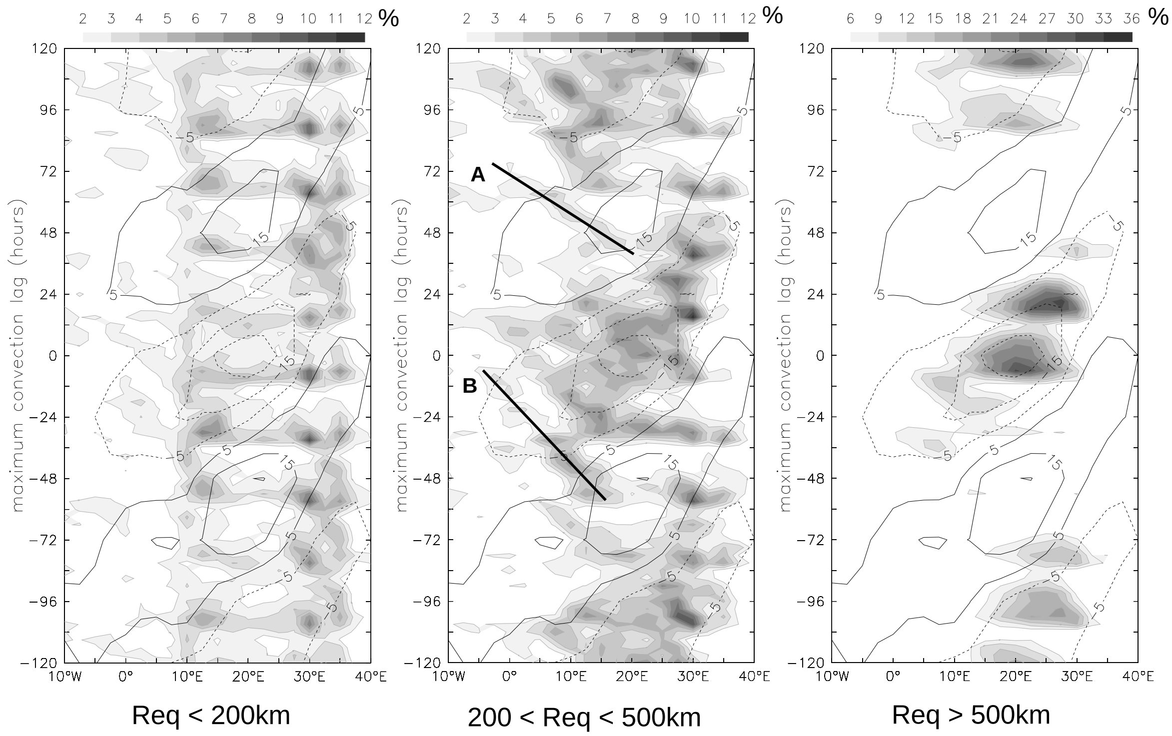


Figure 10: As in figure 9 but for the percentage of pixels over the Congo basin covered by MCS with equivalent radius (a) smaller than 200 km, (b) between 200-500 km and (c) greater than 500 km (shadings in %).

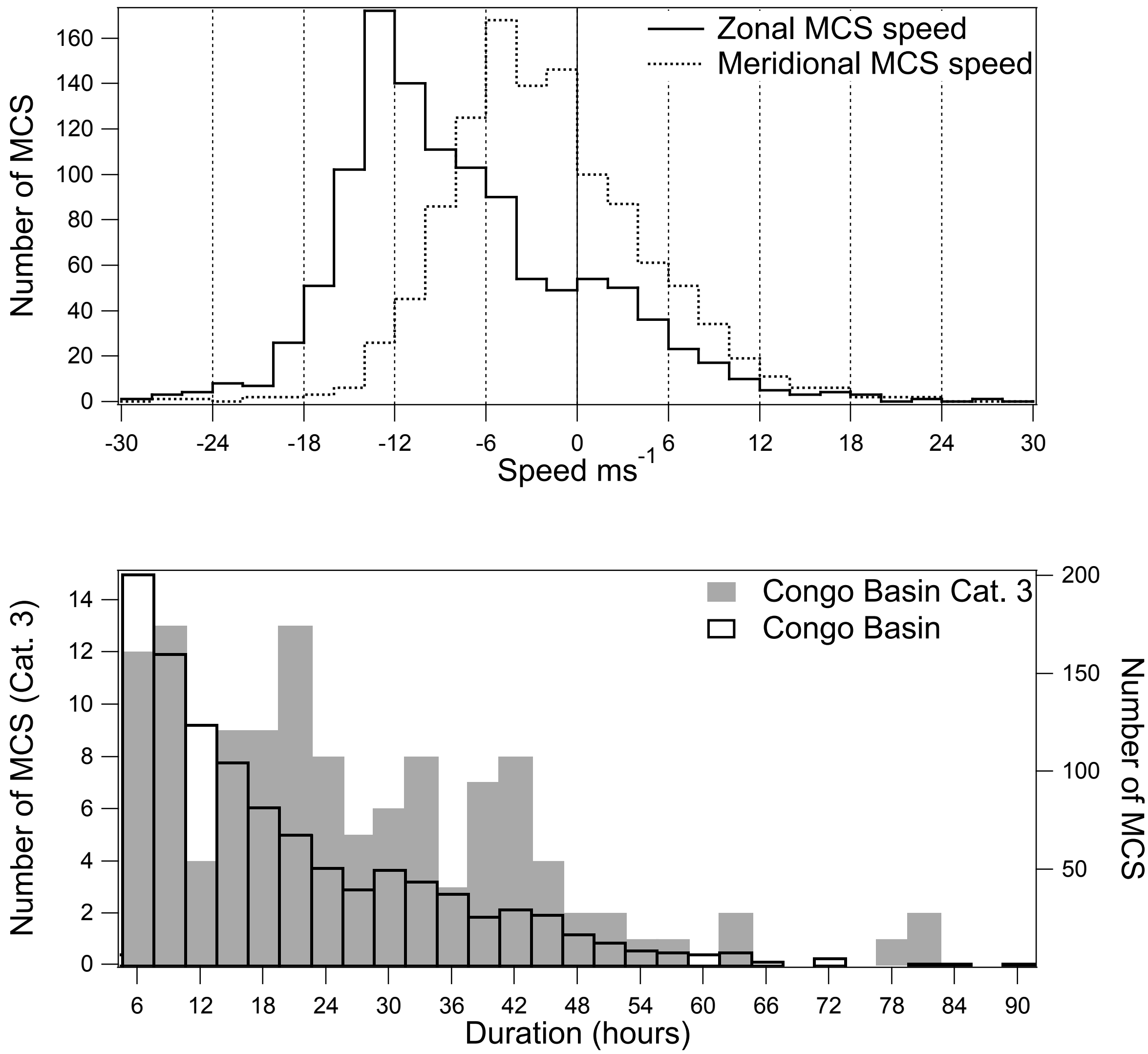


Figure 11: (Top) Distribution of average zonal and meridional speed for convective systems having their center of mass over the Congo basin at least once during their existence. (Bottom) Distribution of the duration of these systems, either for all systems or only for those being over the Congo basin in wave category 3.

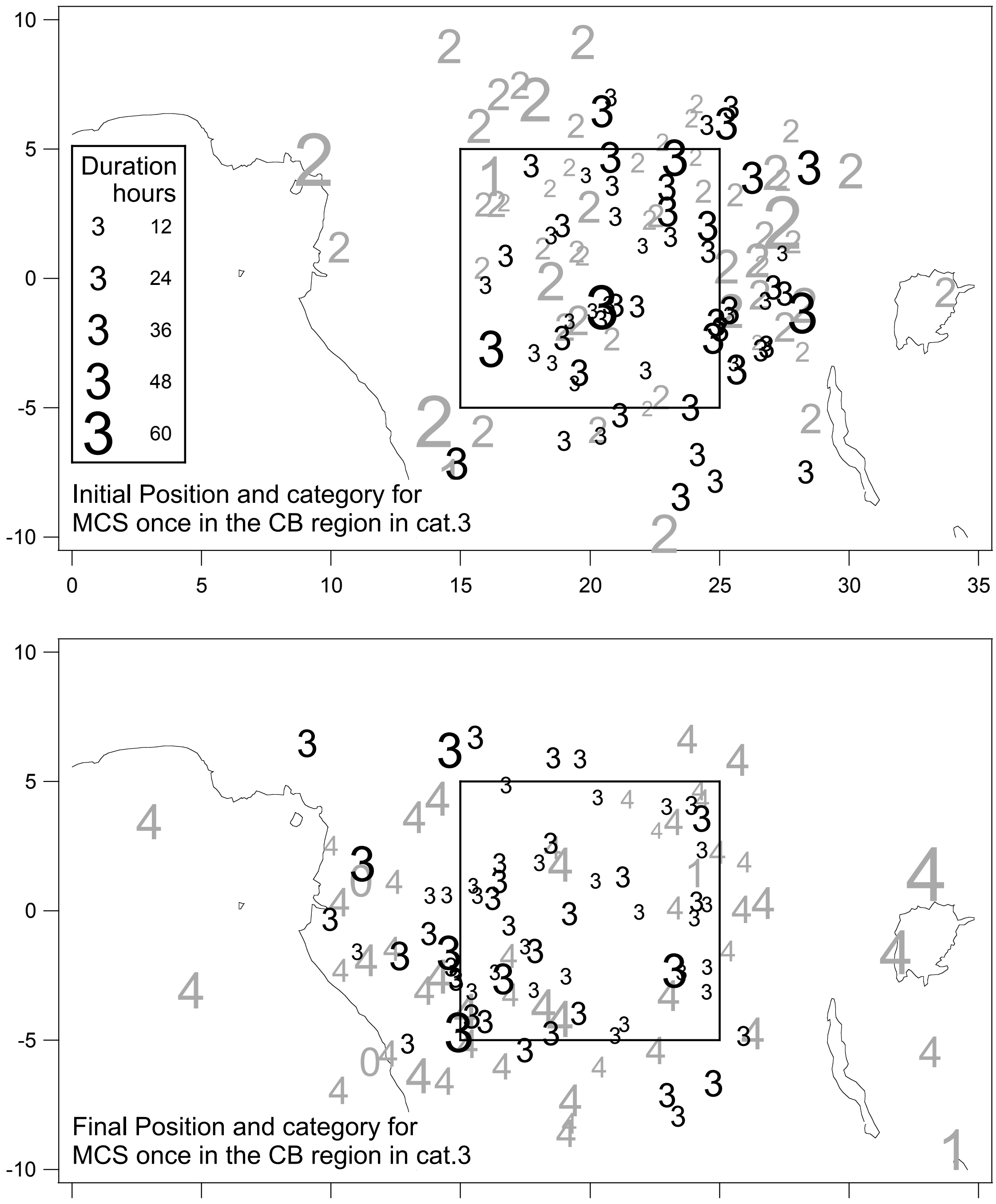


Figure 12: Wave category (1 to 4) and (top) initial and (bottom) final positions of convective systems having their center of mass over the Congo basin in wave category 3 at least once during their existence. The size of the marker is proportional to the duration of the corresponding convective systems.